




Article

Polymeric Nanocapsule Enhances the Peroxidase-like Activity of Fe₃O₄ Nanozyme for Removing Organic Dyes

Junqi Zha ^{1,†}, Wugao Wu ^{1,†}, Peng Xie ¹, Honghua Han ¹, Zheng Fang ^{2,*} , Yantao Chen ^{1,*}  and Zhongfan Jia ^{3,*} 

¹ Shenzhen Key Laboratory of Environmental Chemistry and Ecological Remediation, College of Chemistry and Environmental Engineering, Shenzhen University, Shenzhen 518060, China; junqi-zha@139.com (J.Z.); wuwugao322@163.com (W.W.); x13534293823@126.com (P.X.); hanhscw@163.com (H.H.)

² State Key Laboratory of New Textile Materials & Advanced Processing Technology, School of Materials Science and Engineering, Wuhan Textile University, Wuhan 430200, China

³ Institute for Nanoscale Science and Technology, College of Science and Engineering, Flinders University, Bedford Park, SA 5042, Australia

* Correspondence: 2019077@wtu.edu.cn (Z.F.); ytchen@szu.edu.cn (Y.C.); zhongfan.jia@flinders.edu.au (Z.J.)

† These authors contributed equally to this work.

Abstract: Peroxidase-like nanozymes are nanoscale materials that can closely mimic the activity of natural peroxidase for a range of oxidation reactions. Surface coating with polymer nanogels has been considered to prevent the aggregation of nanozymes. For a long time, the understanding of polymer coating has been largely limited to its stabilization effect on the nanozyme in aqueous media, while little is known about how polymer coating plays a role in interaction with substrates and primary oxidants to dictate the catalytic process. This work reported a facile sequential modification of Fe₃O₄ nanoparticles to polyacrylamide coated nanozymes, and as low as 112 mg/L samples with only 5 mg/L Fe₃O₄ could nearly quantitatively (99%) remove a library of organic dyes with either H₂O₂ or Na₂S₂O₈ as primary oxidants. The catalytic results and molecular simulation provide both experimental and computational evidence that the hydrogen bonding interaction between the reactant and nanozymes is key for the high local concentration hence catalytic efficiency. We envision that this work, for the first time, provides some insights into the role of polymer coating in enhancing the catalytic activity of nanozyme apart from the well-known water dispersity effect.

Keywords: polymeric nanocapsule; Fe₃O₄ nanoparticle; nanozyme; peroxidase-like activity; advanced oxidation processes; organic pollutant



Citation: Zha, J.; Wu, W.; Xie, P.; Han, H.; Fang, Z.; Chen, Y.; Jia, Z.

Polymeric Nanocapsule Enhances the Peroxidase-like Activity of Fe₃O₄ Nanozyme for Removing Organic Dyes. *Catalysts* **2022**, *12*, 614. <https://doi.org/10.3390/catal12060614>

Academic Editor: Aniello Costantini

Received: 20 April 2022

Accepted: 29 May 2022

Published: 3 June 2022

Publisher's Note: MDPI stays neutral with regard to jurisdictional claims in published maps and institutional affiliations.



Copyright: © 2022 by the authors. Licensee MDPI, Basel, Switzerland. This article is an open access article distributed under the terms and conditions of the Creative Commons Attribution (CC BY) license (<https://creativecommons.org/licenses/by/4.0/>).

1. Introduction

Advanced oxidation processes (AOPs), producing highly oxidative hydroxyl radicals that react with persistent organic pollutants, have become a popular technique for wastewater remediation [1]. Among various AOPs, the Fenton process, in which Fe²⁺ triggers a decomposition of H₂O₂ into hydroxyl radicals, has attracted significant attention due to its simplicity, diverse applications, and easy operation of the reaction system [2]. Fe²⁺ could be replaced by Fe³⁺ or other transition metal ions and result in a similar process. Fenton or Fenton-like reactions produce a high concentration of hydroxyl radicals when using hydrogen peroxide as the primary oxidant [3]. These highly reactive hydroxyl radicals are responsible for further reactions involving a radical process, such as radical polymerization and pollutant degradation. However, the traditional Fenton process shows a low efficiency in generating hydroxyl radicals from hydrogen peroxide (<30%), therefore requiring the addition of a large amount of H₂O₂ (30~6000 mM) and Fe²⁺ (18~410 mM) [4]. While a high concentration of Fe²⁺ can easily form an iron slurry, leading to the toxicity of the catalyst, the system also incurs a high cost.

Nanozymes are nanomaterials that display enzyme-like reactivity but can overcome the limitations of natural enzymes, including high cost and poor stability upon changing the reaction and storage environment [5]. Recently, using metallic compounds as

nanozymes represents a viable strategy to remove organic pollutants [6]. Firstly reported by Yan and coworkers in 2007, the ferromagnetic Fe_3O_4 nanoparticles have shown intrinsic peroxidase-like catalytic activity that could activate hydrogen peroxide and produce hydroxyl radicals, leading to the oxidization of multiple substrates [7]. Their high specific surface area and excellent stability make nanoparticles expose much more active sides during the reaction and thus can simultaneously transfer more electrons in the catalysis process. Other than Fe_3O_4 nanoparticles, many other metal nanoparticles, such as FeS [8], CuFe_2O_4 [9], CeO_2 [10], MnO_2 [11], CdS [12], and $\text{CuO-Fe}_3\text{O}_4$ [13] have demonstrated a similar peroxidase-like activity as Fe_3O_4 . These nanozymes can efficiently oxidize and remove organic pollutants when mixed with hydrogen peroxide [14], peroxymonosulfate [9,15], or persulfate [8,16,17]. Interestingly, the Fe_3O_4 nanozyme can activate both hydrogen peroxide and peroxymonosulfate and persulfate [18]. Among the available non-noble metal oxide or sulfide nanoparticles, Fe_3O_4 nanoparticles stand out as an ideal catalyst due to their minimum environmental footprint, cost-effectiveness, easy access and simple separation and recycling by an external magnetic field. Unfortunately, the organic pollutants and oxidized products can also bind to the surface of nanozymes, and block the active sites, leading to the aggregation of nanoparticles and the drastic attenuation of its enzyme-like activity.

Surface modification is a potential method to inhibit aggregation and maintain the stability of Fe_3O_4 nanoparticles [19]. For example, Fe_3O_4 coated with dopamine could afford nanoparticles with better water dispersibility than the naked Fe_3O_4 nanoparticles [20]. Polydopamine has also been coated on the surface of Fe_3O_4 microspheres to assist the immobilization of Ag nanoparticles on the surface of Fe_3O_4 microspheres, resulting in fast adsorption of a model dye methylene blue (MB) [21]. Glutathione-coated Fe_3O_4 nanoparticles exhibited enhanced peroxidase-like activity for oxidizing 2,4-dichlorophenol [14]. Moreover, with the help of molecularly imprinted polymers, Liu and collaborators recently created substrate-binding pockets on the surface of Fe_3O_4 nanozymes, showing a nearly 100-fold enhancement in the substrate selectivity compared to the bare Fe_3O_4 [22]. While these studies provide evidence that surface modification of nanozymes with polymers could prevent aggregation and improve substrate selectivity, little is known about how the polymer layers interact with organic substrates, hence promoting the catalytic process.

In this work, we proposed a facile method for preparing monodisperse Fe_3O_4 nanozymes with excellent water dispersity via the classic dopamine coating and in situ polymer encapsulation. The prepared samples showed enhanced peroxidase-like activity and achieved the purpose of removing organic dyes. Importantly, we successfully employed molecular simulation methods to study the interaction and diffusion of substrates into the polymer coating, demonstrating a coordination effect of organic dyes, persulfates, and amino groups from polymers. This provided some important insights into the selection of appropriate polymers for nanozyme modification toward disparate application scenarios.

2. Results

2.1. Design and Synthesis of $\text{Fe}_3\text{O}_4@\text{Gel}$

Here, the oleic acid-coated nanoparticles were referred to as OA- Fe_3O_4 . The alkane chains of OA are helpful for Fe_3O_4 nanoparticles to be dispersed in non-polar solvents, such as n-hexane. On the other hand, dopamine (DA) could assist Fe_3O_4 NPs dispersion in polar solvents, such as methanol or water. In this work, we coated Fe_3O_4 nanoparticles with dopamine through a phase-transfer process from the n-hexane phase to the methanol phase (Figure 1B). The obtained nanoparticle in methanol is referred to as DA- Fe_3O_4 . DA has also been used to directly coat the Fe_3O_4 nanoparticles in an alkaline solution [21,23]. The driving force for such a phase-transfer process was attributed to the strong interaction with Fe_3O_4 exerted by DA. The hydroxyl groups and amide groups of dopamine endow hydrophilic to the surface of Fe_3O_4 nanoparticles and ensure their aqueous dispersibility. The averaged hydrodynamic diameter of DA- Fe_3O_4 was about 24.4 nm, as determined by DLS in Figure 2A. However, serious aggregation and precipitation of DA- Fe_3O_4 still

appeared after three-day storage in an aqueous solution (pH = 7) as the naked Fe_3O_4 (see Figure 1C).

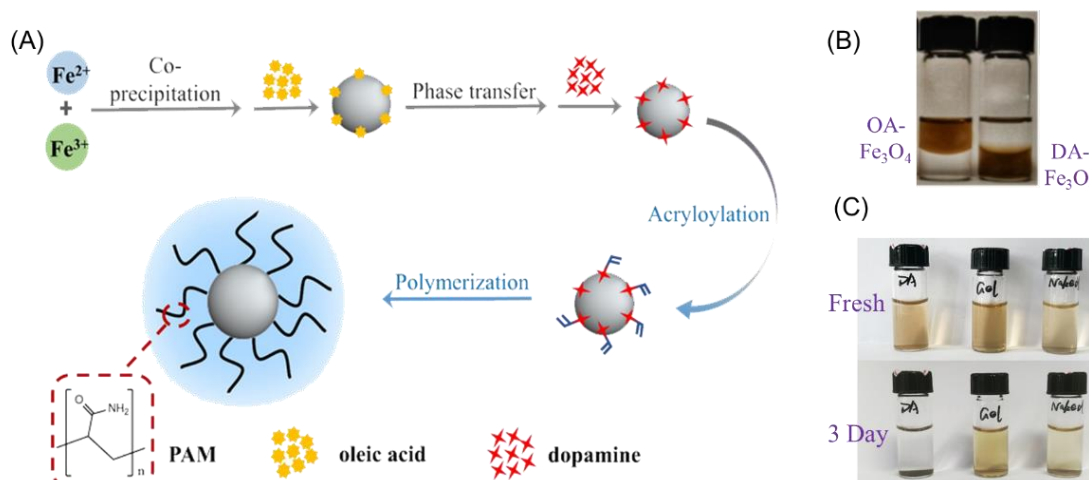


Figure 1. (A) Schematic illustration for preparing the water-dispersible Fe_3O_4 nanoparticles via polymeric encapsulation ($\text{Fe}_3\text{O}_4@\text{Gel}$). (B) Nanoparticle samples dispersed in n-hexane and methanol, respectively ($\text{OA-Fe}_3\text{O}_4$ & $\text{DA-Fe}_3\text{O}_4$); (C) Nanoparticle samples freshly prepared and after three days of storage in an aqueous solution.

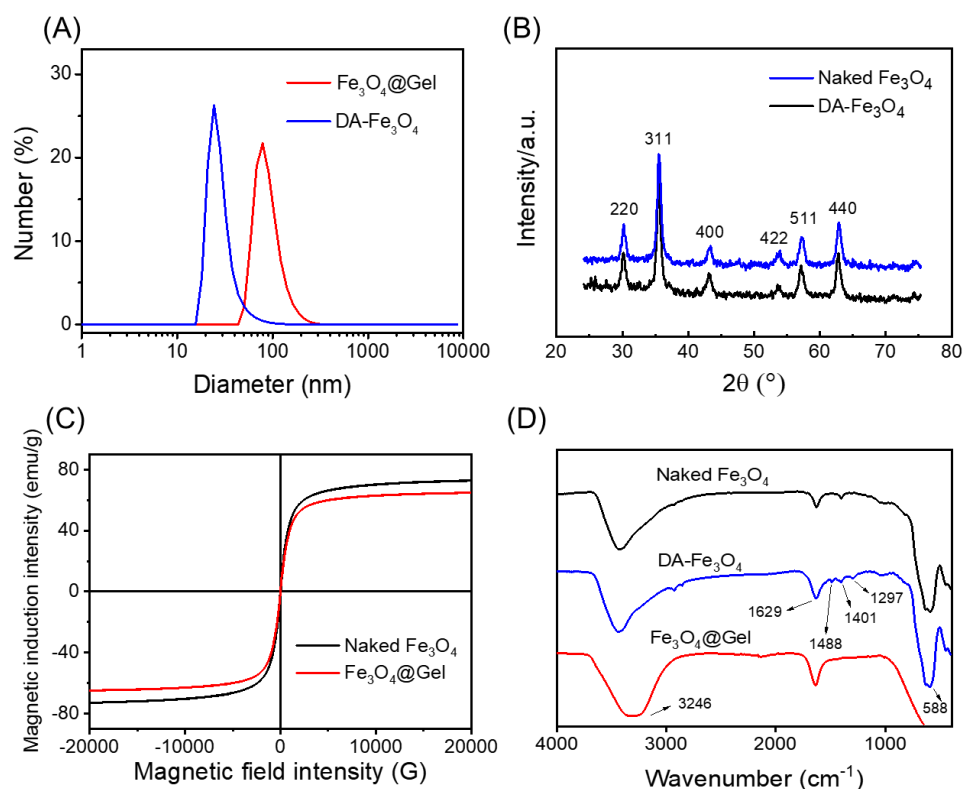


Figure 2. Physical characterization of the naked Fe_3O_4 , $\text{DA-Fe}_3\text{O}_4$, and $\text{Fe}_3\text{O}_4@\text{Gel}$. (A) Size distribution measured by DLS; (B) XRD patterns; (C) Magnetization curves; (D) FT-IR spectra.

To tackle this problem, we further performed a chemical modification to encapsulate $\text{DA-Fe}_3\text{O}_4$ nanoparticles into a thin polymer layer. The amino groups of dopamine coating on $\text{DA-Fe}_3\text{O}_4$ NPs were chemically modified with acryloyl groups and then copolymerized with AAM monomer. The polymerization formed a porous hydrogel layer that covered $\text{DA-Fe}_3\text{O}_4$ NPs. Hereafter, the Fe_3O_4 embedded nanogel/nanocapsule is referred to as

$\text{Fe}_3\text{O}_4@\text{Gel}$. As shown in Figure 1C, $\text{Fe}_3\text{O}_4@\text{Gel}$ was stable during three-day storage in an aqueous solution, and its hydrodynamic diameter was about 78.8 nm (see Figure 2A). We can imagine that the aggregation of Fe_3O_4 nanoparticles should be effectively inhibited after polymeric encapsulation. Notably, the corresponding peaks for DA- Fe_3O_4 totally disappeared in the diameter distribution of $\text{Fe}_3\text{O}_4@\text{Gel}$, indicating that all DA- Fe_3O_4 nanoparticles should be encapsulated into polymeric nanogel.

2.2. Physical Characterization of Samples

Except for the hydrodynamic diameter in an aqueous solution, more characterizations were carried out for the three Fe_3O_4 samples. In the X-ray diffraction (XRD) pattern of naked Fe_3O_4 and DA- Fe_3O_4 (see Figure 2B), Miller indices with strong response peaks were 220, 311, 400, 440, and 511, respectively. Such patterns were well-matched with the standard Fe_3O_4 (JCPDS no. 19-0629) [14], indicating high purity and good crystalline morphology for the surface-modified DA- Fe_3O_4 .

The vibration sample magnetometer behavior of naked Fe_3O_4 and $\text{Fe}_3\text{O}_4@\text{Gel}$ were measured. As shown in Figure 2C, the saturation magnetic induction of naked Fe_3O_4 was 72.8 emu/g, and slowly decreased to 64.9 emu/g after encapsulation in polymer nanogel but was still greater than 16.3 emu/g [24]. Such larger values verified that dopamine modification and polymeric encapsulation exerted little influence on the magnetic property of Fe_3O_4 nanoparticles.

The functional groups of the surface-modified Fe_3O_4 samples have also been characterized by FT-IR spectroscopy (Figure 2D). The Fe-O stretching vibration was near 588 cm^{-1} , a typical absorption band for Fe_3O_4 . Compared with naked Fe_3O_4 , some new absorption bands appeared in the infrared spectrum of DA- Fe_3O_4 . The narrow peak located at 1488 cm^{-1} was attributed to the C=C vibration of the benzene ring, and the peak located at 1297 cm^{-1} can be attributed to the C=O stretching of the phenolic hydroxyl group validating the successful preparation of DA- Fe_3O_4 [20]. For the sample $\text{Fe}_3\text{O}_4@\text{Gel}$, the broad peak occurring between 3500 and 3200 cm^{-1} corresponds to hydrogen-bonded O-H stretching. The increased intensity of the peak at 1629 cm^{-1} indicated the collective signals from the aromatic ring of DA, N-H bends, and C=O stretches of amide bonds of the polymer layer.

The dried sample of $\text{Fe}_3\text{O}_4@\text{Gel}$ was further characterized by TEM. As shown in Figure 3, the diameter of $\text{Fe}_3\text{O}_4@\text{Gel}$ was estimated between 10 nm and 20 nm. The high-resolution TEM image in Figure 3C displays a crystal lattice fringe with about 0.25 nm, fitting well with the cubic structure Fe_3O_4 (311) planes [14,25]. As the dried polymer nanocapsule formed a thin film around the Fe_3O_4 surface and resulted in a slight aggregation of the samples. Careful observation reveals that the $\text{Fe}_3\text{O}_4@\text{Gel}$ samples presented a core-shell morphology with the inner Fe_3O_4 core (dark grey) and the outer polymer layer (light grey). Moreover, the elemental mapping (Figure S1 in Supplementary Materials) demonstrates that the Fe elements were in the core area while the N elements were in the shell area, unambiguously indicating the core-shell structure of $\text{Fe}_3\text{O}_4@\text{Gel}$ nanoparticles.

2.3. Peroxidase-Mimicking Activity of $\text{Fe}_3\text{O}_4@\text{Gel}$

The Fe_3O_4 nanoparticles could catalytically oxidize peroxidase substrates in company with H_2O_2 , exhibiting a peroxidase-like activity as firstly reported by the Yan group [7]. In this work, the peroxidase-like activities of modified Fe_3O_4 samples were evaluated according to the catalytic oxidation of TMB, a peroxidase chromogenic substrate. As shown in Figure 4A, DA- Fe_3O_4 exhibited improved peroxidase-mimicking activity, ca. 2.7-times of naked Fe_3O_4 nanoparticles. Since the naked Fe_3O_4 nanoparticles were prepared without oleic acid or dopamine, their lower catalytic degradation ability suggested that dopamine was conducive to the preparation of water-dispersed Fe_3O_4 nanoparticles, which could effectively enhance its catalytic performance. After polymer encapsulation, the enzymatic performance was further increased to ca. 3.1 times of naked Fe_3O_4 nanoparticles. As a comparison, the polymeric nanogel exhibited no significant enzymatic activity. Intuitively, the polymer nanogel seems to prevent the diffusion of organic substrates to the nanozyme

centers. However, the results suggested that the permeability of the porous polymeric layer is good enough to allow the free diffusion of substrates and hydrogen peroxide molecules. In our previous work on encapsulating horseradish peroxidase (HRP), the low Michaelis-Menten constant and high catalytic efficiency validated the good permeability for the free diffusion of substrate molecules into the enzyme active site [26,27].

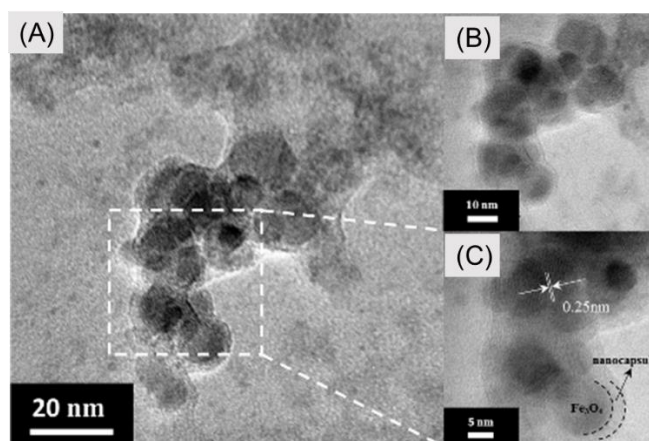


Figure 3. TEM images of $\text{Fe}_3\text{O}_4@\text{Gel}$ nanoparticles (A,B) and the enlarged nanoparticles showing the polymer layer (C) with an average diameter of 12.0 ± 2.8 nm. The accelerated voltage was 80 kV.

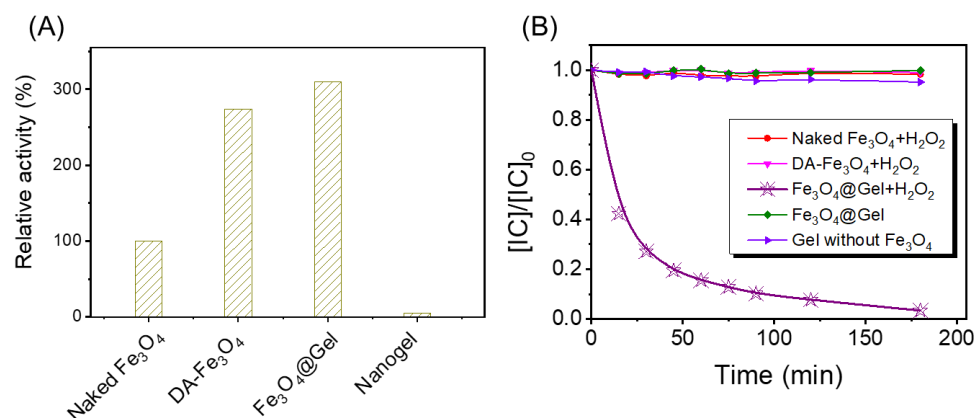


Figure 4. Peroxidase mimic activities of Fe_3O_4 samples based on the oxidation of TMB (A) and IC (B). Reaction conditions: $[\text{H}_2\text{O}_2]_0 = 20$ mM, $[\text{Fe}_3\text{O}_4] = 5$ mg/L, $[\text{TMB}]_0 = 200$ mg/L, $[\text{IC}]_0 = 200$ mg/L, pH = 7, and $T = 30$ °C.

2.4. Efficient Removal of Organic Dyes with H_2O_2

Next, we explored the effect of polymeric encapsulation on the catalytic performance of Fe_3O_4 on organic dyes. Indigo carmine (IC) was chosen as another target for catalytic oxidation. As shown in Figure 4B, in the IC/ H_2O_2 mixed solution, IC can be rapidly degraded with the addition of $\text{Fe}_3\text{O}_4@\text{Gel}$; the removal efficiency was as high as 57.6% after 15 min and 99% after 180 min. In comparison, there is almost no IC degradation after the addition of naked Fe_3O_4 , DA- Fe_3O_4 , or nanogel without Fe_3O_4 . As aforementioned, the peroxidase-mimicking activity of DA- Fe_3O_4 and $\text{Fe}_3\text{O}_4@\text{Gel}$ were very similar when oxidating TMB. In our opinion, this can be rationalized by the adsorption effect between the polymeric nanogel and dyes. The nanogel is composed of polyacrylamide, which is rich in amide groups. Each IC molecule contains two sulfonic acid groups and thus could be adsorbed into the nanogel through hydrogen bonding. As shown in Figure 5A, the increased local concentration of IC inside the gel increased the oxidation reaction rate.

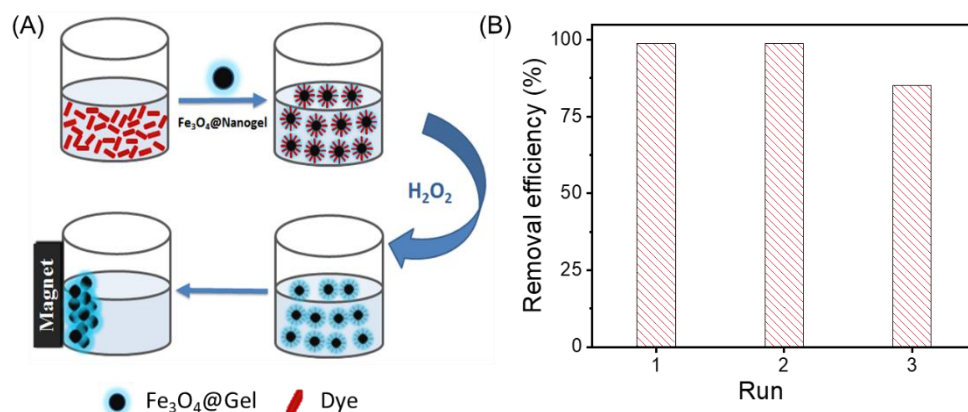


Figure 5. (A) Reusability of Fe₃O₄@Gel as illustrated by sketch map. (B) Variation of removal efficiency of IC when catalyzed by the reused Fe₃O₄@Gel. Reaction conditions: [H₂O₂] = 20 mM, [Fe₃O₄] = 5 mg/L, [IC] = 200 mg/L, pH = 7, and $T = 30\text{ }^{\circ}\text{C}$.

Next, the catalytic performance was evaluated with various concentrations of H₂O₂ and Fe₃O₄@Gel. Increasing H₂O₂ could enhance the removal efficiency of IC, and the enhancement became less intense when H₂O₂ was above 20 mM, indicating that the local concentration of H₂O₂ inside the nanocapsules approached saturation (see Figure S2A). Similarly, the saturation concentration of Fe₃O₄@Gel was [Fe₃O₄] = 5 mg/L, and double loading of Fe₃O₄@Gel only increased the removal efficiency from 79.7% to 93.8% (see Figure S2B). In the following studies, the dosage of Fe₃O₄@Gel was fixed at 112 mg/L, which is equivalent to [Fe₃O₄] = 5.0 mg/L.

The magnetic property of Fe₃O₄@Gel could also be used in the effective collection of nanozymes under external magnetic fields (Figure 5). Reuse experiments were performed to evaluate the catalytic sustainability of Fe₃O₄@Gel. It was revealed that more than 85% of IC could still be removed in the third run. Considering the mass loss in recirculation, we can speculate that Fe₃O₄@Gel nanoparticles could be a good choice in the continuous treatment of wastewater. In contrast, the catalytic performance of the Fe₃O₄ nanoparticles recycled three times is only 40% of the fresh sample when oxidizing acetaminophen [28].

2.5. Efficient Removal of Organic Dyes with Na₂S₂O₈

Other than H₂O₂, Na₂S₂O₈ can also supply free radicals in the advanced oxidation process. Here, another catalytic oxidation system was constructed based on Na₂S₂O₈ in company with Fe₃O₄@Gel. As shown in Figure 6, IC can be fully removed by both Fe₃O₄@Gel/H₂O₂ and Fe₃O₄@Gel/Na₂S₂O₈, while a remarkable difference is displayed in the oxidation of other dyes, i.e., AO7, DR81, and AZO. The oxidation performance of Fe₃O₄/Na₂S₂O₈ was significantly higher than that of Fe₃O₄/H₂O₂. This may be attributed to the longer half-life of sulfate radicals ($\bullet\text{SO}_4^-$), supplying a higher probability of encountering and oxidizing dye molecules before quenching. Nevertheless, the polymer encapsulation significantly enhanced the catalytic oxidation performance of the Fe₃O₄ nanozyme, regardless of the primary oxidants H₂O₂ or Na₂S₂O₈. Especially when oxidizing AZO, the removal efficiency was improved by 77%. Considering that all dyes in this work (i.e., IC, AO7, DR81, and AZO) contain sulfonic acid groups, the polymeric nanocapsules should be able to adsorb these dyes, thereby improving their catalytic oxidation efficiency.

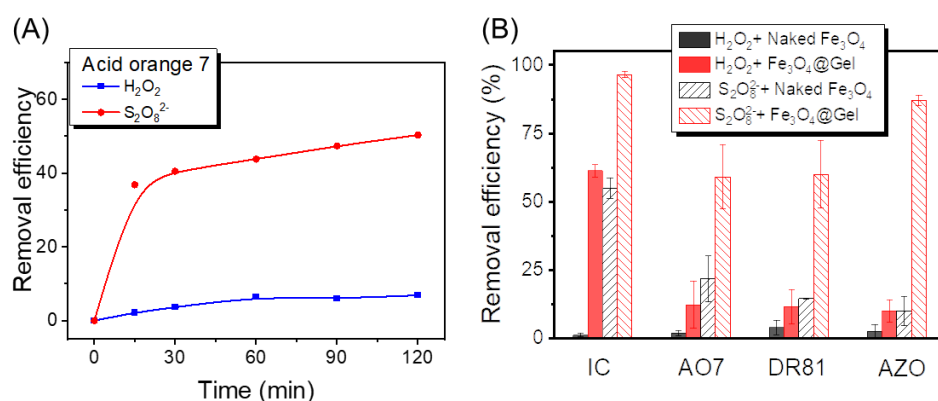


Figure 6. Comparison of the catalytic performance between the $\text{Fe}_3\text{O}_4/\text{H}_2\text{O}_2/\text{dye}$ system and the $\text{Fe}_3\text{O}_4/\text{Na}_2\text{S}_2\text{O}_8/\text{dye}$ system. (A) Removal efficiencies as functions of elapsed time; (B) Removal efficiencies of dyes after oxidized for two hours. Reaction parameters: $[\text{Na}_2\text{S}_2\text{O}_8]_0 = 10 \text{ mM}$, $[\text{H}_2\text{O}_2]_0 = 10 \text{ mM}$, $[\text{Fe}_3\text{O}_4] = 5.0 \text{ mg/L}$, $[\text{dye}]_0 = 100 \text{ mg/L}$, $\text{pH} = 7.0$, and $T = 30^\circ\text{C}$.

The catalytic performance was also evaluated with different loading of $\text{Na}_2\text{S}_2\text{O}_8$ and $\text{Fe}_3\text{O}_4@\text{Gel}$, and various pH. As shown in Figure S3, $\text{Fe}_3\text{O}_4@\text{Gel}$ showed the best degradation efficiency of AO7 when $\text{pH} = 7$; the degradation was slightly weakened in the alkaline environment, and was only 20% in the acidic environment, especially at $\text{pH} = 4$. Furthermore, Figure S4 shows that increasing $\text{Na}_2\text{S}_2\text{O}_8$ could also enhance the removal efficiency of AO7, indicating that the local saturation concentration of $\text{Na}_2\text{S}_2\text{O}_8$ inside the nanocapsules should be about 10 mM. Similarly, the plateau concentration of $\text{S}_2\text{O}_8^{2-}$ was close to that of H_2O_2 when using $\text{Fe}_3\text{O}_4@\text{Gel}$. Notably, Fenton or Fenton-like systems often used a different design of the catalysts and reaction conditions, which could be difficult for a direct comparison. As such, we have listed the catalysis performance of previous work, from which one could have a better understanding of the pros and cons of each system (Table S1).

2.6. Identification of Primary Reactive Oxidants

The catalytic degradation is usually through a radical mechanism. To identify the types of radicals in our systems, we performed EPR experiments by adding the spin-trapping agent DMPO. It is known that the Fenton reaction generates hydroxyl radicals ($\bullet\text{OH}$) from H_2O_2 , whereas the $\bullet\text{SO}_4^-$ is produced from the decomposition of $\text{Na}_2\text{S}_2\text{O}_8$. As illustrated in Figure 7B, the characteristic quartet peak with an intensity ratio of 1:2:2:1 indicated large quantities of DMPO-OH adducts in the $\text{Fe}_3\text{O}_4@\text{Gel}/\text{H}_2\text{O}_2$ system. In contrast, the obvious signals of both DMPO-OH (1:2:2:1) and DMPO- SO_4 (1:1:1:1:1:1) appeared for the $\text{Fe}_3\text{O}_4@\text{Gel}/\text{Na}_2\text{S}_2\text{O}_8$ system, suggesting an in situ conversion of $\bullet\text{SO}_4^-$ to $\bullet\text{OH}$ [16,28].

The highly reactive hydroxyl radicals are supposed to initiate the degradation reaction of the substrates. Deactivation of quenching these radicals with more radical-reactive species should then inhibit the degradation reaction. To prove this hypothesis, we took the $\text{Fe}_3\text{O}_4@\text{Gel}/\text{H}_2\text{O}_2$ system as an example by adding *tert*-butanol (TBA) as a typical hydroxyl radical ($\bullet\text{OH}$) scavenger. As depicted in Figure 7A, the concentration of IC decreased quickly, and the removal efficiency was as high as 73% after 150 min. As the amount of TBA increased from 1 mM to 8 mM, the degradation process of IC was significantly inhibited, and the removal efficiency decreased from 65% to 11%. These data agreed with the fact that hydroxyl radicals are direct oxidants to the substrates, and almost all the hydroxyl radicals were scavenged when the concentration of TBA exceeds 5 mM [29].

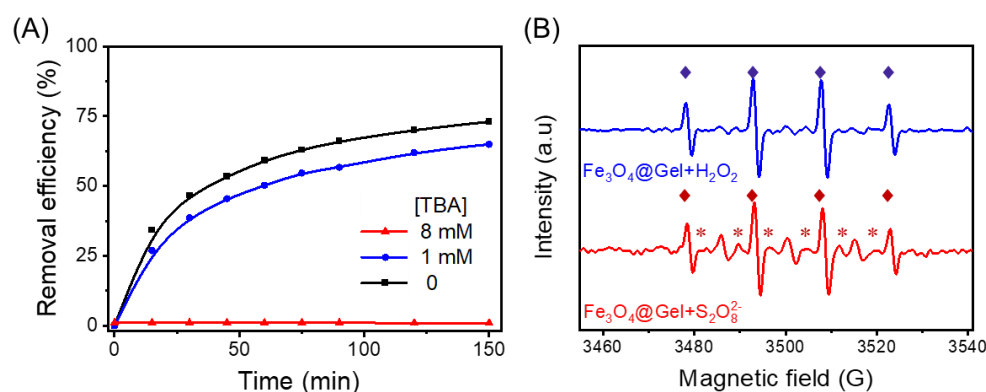


Figure 7. (A) Effect of TBA on the degradation of IC in the $\text{Fe}_3\text{O}_4@\text{Gel}/\text{H}_2\text{O}_2$ system; (B) EPR spectrum of $\text{DMPO}\cdot\text{OH}$ adduct (♦) and $\text{DMPO}\cdot\text{SO}_4^-$ adduct (*) in the $\text{Fe}_3\text{O}_4@\text{Gel}/\text{H}_2\text{O}_2$ and $\text{Fe}_3\text{O}_4@\text{Gel}/\text{Na}_2\text{S}_2\text{O}_8$ systems, respectively.

2.7. An Adsorption Mechanism as Revealed by Molecular Simulation

Our previous work [30] revealed that the molecular interactions between the PAM nanogel and the dye (AZO) enable the dye molecules to be efficiently absorbed into the nanogel interior. In this work, IC was chosen as the model dye, and acrylamide tetramers were used to represent the PAM nanocapsule. Using molecular simulations, we compared the intermolecular interactions existing in two typical systems, i.e., the $\text{PAM}/\text{H}_2\text{O}_2/\text{IC}$ system and the $\text{PAM}/\text{Na}_2\text{S}_2\text{O}_8/\text{IC}$ system. The three components in the simulated system were first randomly placed inside the simulation box and then aggregated, driven by molecular interactions. The number of atomic contacts between every two components was used to track the aggregating process.

As presented in Figure 8, the number of atomic contacts between dye and $\text{H}_2\text{O}_2/\text{Na}_2\text{S}_2\text{O}_8$ was the most among all the formed contacts, which increased and then approached a plateau after about 20 ns. This means that the simulated system reached the thermodynamic equilibrium after 20 ns. Several insights could be obtained from the simulation results. In the $\text{PAM}/\text{H}_2\text{O}_2/\text{IC}$ system, the number of atomic contacts between PAM and IC increased rapidly and reached its equilibrium value of 5960 after 15 ns, indicating a strong interaction between PAM and IC. In other words, the interaction between H_2O_2 and PAM was much weaker, and the number of associated atomic contacts was only 2041. Given that the large number of atomic contacts formed between IC and H_2O_2 was ca. 15,023, H_2O_2 should also be largely absorbed into the nanocapsule. As illustrated in Figure 9, IC was the key in the adsorption process, which can interact with PAM and H_2O_2 to promote aggregation of the three components, increasing the local concentration of IC and H_2O_2 inside the nanocapsule. Considering that the concentrations of organic pollutants are very low (<1000 ppm) in wastewater, hydroxyl radicals cannot capture the organic pollutants during their short lifetime (ca. 1 μs) [31] via free diffusion. In the PAM nanocapsule, the locally concentrated dye and H_2O_2 were endowed with increased possibilities to be oxidized by hydroxyl radicals.

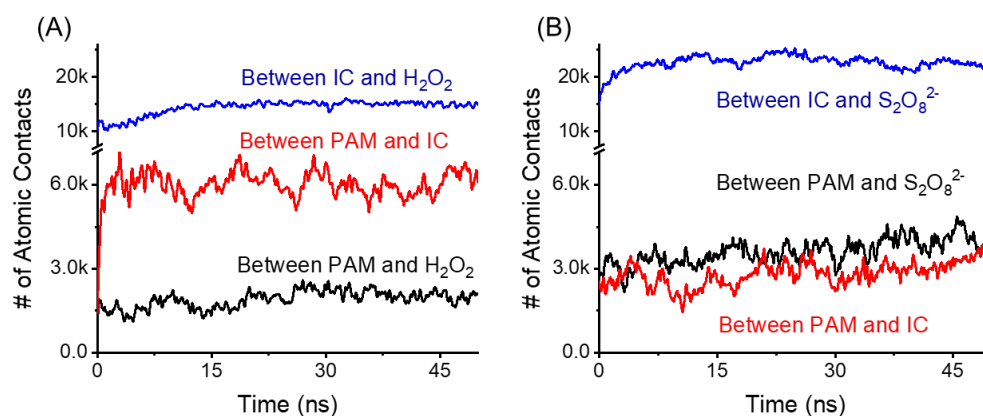


Figure 8. Time evolution of the simulated system as revealed by two order parameters. They are the number of atomic contacts (A) and hydrogen bonds (B) between different components, i.e., polymeric gel (PAM), dye (IC), and H₂O₂.

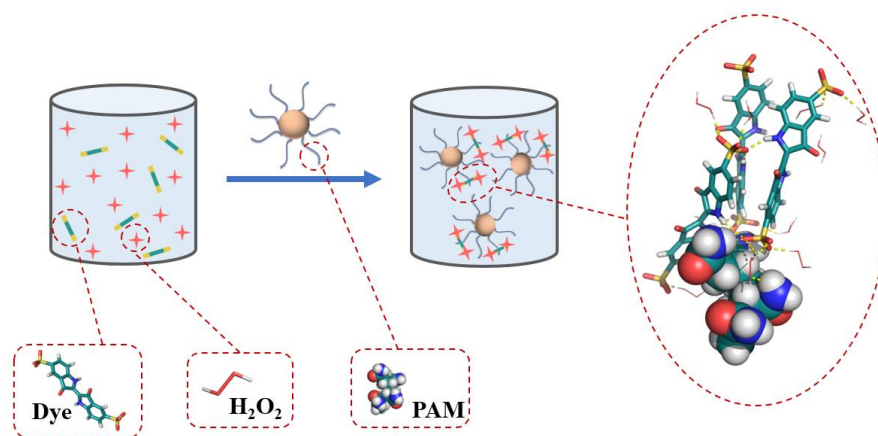


Figure 9. A proposed mechanism for the enhanced removal of dye pollutants via a combination of adsorption and catalytic oxidation. The yellow dashed line denoted the hydrogen bonds formed between PAM, dye, and H₂O₂.

In the PAM/Na₂S₂O₈/IC system, the number of atomic contacts between Na₂S₂O₈ and IC increased rapidly and reached its plateau value (ca. 22,257) after 20 ns, indicating that the stronger intermolecular interactions were formed between the secondary ammonia of IC and Na₂S₂O₈, such as hydrogen bonding. In contrast, the number of atomic contacts between PAM and IC was only 3154, which is about one-half of that in the PAM/H₂O₂/IC system. Considering that the number of atomic contacts between PAM and Na₂S₂O₈ was 4025, significantly larger than that between PAM and H₂O₂ in the PAM/H₂O₂/IC system, we suppose that Na₂S₂O₈ formed stronger hydrogen bonding with the primary ammonia of PAM, thus decreased the adsorption between PAM and IC. The three components in the PAM/Na₂S₂O₈/IC system can interact with each other, which is conducive to aggregation or adsorption. In contrast, H₂O₂ in the PAM/H₂O₂/IC system requires the assistance of IC to enter the nanocapsules. This also rationalizes the stronger oxidizing and removing efficiency of Na₂S₂O₈ on organic dyes in Figure 6.

3. Materials and Methods

3.1. Materials

Ferrous chloride tetrahydrate (FeCl₂·4H₂O, 99.95%), ferric chloride (FeCl₃·6H₂O, 99%), Oleic acid (OA, 99%) acrylamide monomer (AAM), N-acryloxysuccinimide (NAS), ammonium persulfate (APS), tetramethylethylenediamine (TEMED), 3,3',5,5'-Tetramethylbenzidine dihydrochloride (TMB), 5,5-dimethyl-1-pyrroline N-oxide (DMPO), hydrogen peroxide

(30%) and sodium persulfate ($\text{Na}_2\text{S}_2\text{O}_8$) were obtained from Sigma-Aldrich Co. (Shanghai, China) Ammonia water ($\text{NH}_3 \cdot \text{H}_2\text{O}$, 25–28%), dopamine hydrochloride and all dyes (Indigo carmine, IC; Acid orange 7, AO7; Azophloxine, AZO; Direct Red 81, DR81) were supplied by Aladdin Co. (Shanghai, China) Other chemicals were of analytical grade and were used without further purification.

3.2. Preparation of Fe_3O_4 Nanoparticles

3.2.1. Naked Fe_3O_4 NP

Fe_3O_4 nanoparticles were prepared by a co-precipitation method with minor modifications from previous reports [32,33]. Briefly, $\text{FeCl}_3 \cdot 6\text{H}_2\text{O}$ (2.5 mmol), and $\text{FeCl}_2 \cdot 4\text{H}_2\text{O}$ (1.25 mmol) were dissolved in deoxygenated water (5 mL) to get a homogenous mixture. The mixture was slowly dropped into ammonia water (2%, 25 mL, 90 °C) under vigorous stirring (1500 rpm). After that, oleic acid (0.5 mL) was slowly added to the solution and stirred for at least 10 min. The blackish precipitates were gathered with a permanent magnet, washed by deionized water and anhydrous ethanol several times, and then homogeneously dispersed in n-hexane (10 mL). Hereafter, the Fe_3O_4 nanoparticles coated with oleic acid were denoted as OA- Fe_3O_4 NP in this work.

3.2.2. DA- Fe_3O_4 NP

Dopamine was used to modify the surface of Fe_3O_4 by a phase-transfer method. Typically, 0.64 mL of Fe_3O_4 (0.08 mmol) in n-hexane was mixed with 2 mL of dopamine (0.8 mmol) in anhydrous methanol and then stirred at 1500 rpm for 1 h. The dopamine coated Fe_3O_4 NPs were transferred from the non-polar organic phase to the polar methanol phase, and then gathered and washed with deionized water several times. The obtained Fe_3O_4 NPs coated with dopamine could be well dispersed in water, which was denoted as DA- Fe_3O_4 NPs hereafter.

3.3. Encapsulation of Fe_3O_4 Nanoparticles

To synthesize the Fe_3O_4 -embedded nanogel, DA- Fe_3O_4 NPs were firstly modified to introduce acryloyl groups by reacting surface amide groups with N-acryloxysuccinimide (NAS). The reaction was performed by dissolving DA- Fe_3O_4 (8 mM, 100 μL) into 1 mL deoxygenated water under magnetic stirring (1500 rpm), followed by a dropwise addition of 20 μL NAS DMSO solution (20 mg/mL). The reaction lasted for two hours at room temperature. Subsequently, the acrylated DA- Fe_3O_4 was mixed with a 40 mg AAM aqueous solution (2.5 mL). The Fe_3O_4 -embedded nanogel was synthesized via in situ free radical polymerization with the addition of 4 mg APS as initiator and 15 μL TEMED as a stabilizer. After stirring for another two hours, the reaction mixture was concentrated and then washed with deionized water several times.

3.4. Characterization of Fe_3O_4 Nanoparticles

The morphology of Fe_3O_4 nanoparticles was characterized with a Talos F200 \times transmission electron microscope (TEM; Thermo Fischer, Waltham, MA, USA). Fourier transform infrared spectrometer NICOLET IS10 (FT-IR; Thermo Fischer, USA) was used to detect the chemical structures of naked Fe_3O_4 , DA- Fe_3O_4 , and Fe_3O_4 @Gel nanoparticles. X-ray diffraction (XRD) analysis was obtained in an Empyrean X-ray powder diffractometer (PANalytical, Almelo, Holland). Magnetic properties of Bare Fe_3O_4 and Fe_3O_4 @Gel nanoparticles were examined with a Physical Property Measurement System X-MaxN50 (Quantum Design, San Diego, California, USA). The hydrodynamic diameters of samples were measured using a Zeta Sizer Nano S90 (Malvern, Malvern, UK) after sonicating the aqueous samples for 30 min. Electron paramagnetic resonance (EPR) experiments were performed with DMPO as a spin-trapping agent on an EMX-E spectrometer (Bruker, Karlsruhe, Germany). All the spectroscopic measurements were conducted using a 96-well plate in an Epoch2 microplate reader (BioTek, Winooski, VT, USA).

3.5. Peroxidase-Mimic Activity Assessment

The peroxidase-mimic activity of the samples was measured via a luminescence method [30,34]. Briefly, the peroxidase substrates TMB was used as the subject of the catalytic oxidations, and the oxidated TMB could be detected according to the absorbance at 650 nm. The TMB/H₂O₂ system was prepared by mixing TMB (10 µL, 10 mg/mL), H₂O₂ (64 µL, 30%), and acetic acid-sodium acetate buffer solution (800 µL, pH 3.6). The oxidation reaction was started by adding nanozyme sample (200 µL, [Fe₃O₄] = 74 µg/mL) with stirring at 800 rpm and 30 °C. The color change was recorded for 15 min. The catalytic efficiency can be judged by the rate of forming oxidated TMB.

3.6. Batch Experiments for Dye Degradation

The typical process of using Fe₃O₄@Gel to treat organic dyes in the reactor was as follows: Dyes (200 µL, 5 mg/mL) and H₂O₂ (100 µL, 3%) were added sequentially in PBS buffer solutions (pH = 7.0) with stirring at 800 rpm and 30 °C. Then, the reaction was initiated by the addition of the Fe₃O₄@Gel suspension (200 µL, [Fe₃O₄] = 74 µg/mL) and the final volume was 5 mL. Each degradation process was performed with three replicates. Organic dyes were also degraded by the Fe₃O₄/Na₂S₂O₈ system to degrade organic dyes, and the concentration of Na₂S₂O₈ in the reactor was 10 mM or 0.024 mg/mL. Other conditions remained unchanged from the Fe₃O₄/H₂O₂ system.

Concentrations of dyes in the degradation process were determined by detecting the absorbance of supernatant. The characteristic absorption peaks of dyes IC, DA81, AO7, and AZO are 610, 510, 484, and 508 nm, respectively. The removal efficiency (D , %) of dye could be determined as $D\% = C_0/C_t \times 100\%$, where C_0 is the initial concentration of dye, and C_t represents the concentration after elapsed time t .

3.7. Molecular Modeling and Computer Simulations

The interaction modes at molecular level among nanocapsule, organic dye, and H₂O₂/Na₂S₂O₈ were explored based on all-atom molecular dynamics (AAMD) simulations. As verified in our previous work [30], the repeating unit of polyacrylamide could represent the nanocapsule material to form interactions with other components. Gauss view software (version 5.0, Wallingford, CT, USA) was used to construct the structures of acrylamide tetramers, indigo carmine, H₂O₂, and Na₂S₂O₈, and Automated Topology Builder (ATB) [35] was used to produce the associated topologies. Molecular interactions between each other were described by the GROMOS force field (version 54A8) [36], and water molecules were represented by the classical TIP3P model [37]. The simulated system was composed of 10 acrylamide tetramers, 50 indigo carmine, 200 H₂O₂, or Na₂S₂O₈, these ratios were set following the experimental feeding ratios. To make the solution electrically neutral, sodium ion (Na⁺) and chloride ion (Cl[−]) were added. As the size of the simulation box is 6 nm × 6 nm × 6 nm, periodic boundary conditions were applied in the x-, y-, and z-directions to approximate an infinite environment.

All AAMD simulations were conducted in the isothermal-isobaric (NPT) ensemble using the GROMACS simulation package (version 2018.4) [38] at the National Supercomputing Center in Shenzhen. The simulations were performed with a 2-fs time step at 1 bar and 310 K, and the last 20-ns trajectory was used for data analysis. The PyMOL suite (Schrödinger Co.) [39] was used to visualize the simulated systems. Other details of the simulation can be found in our previous work [30]. The number of atomic contacts between each component of the simulated system was counted via the *gmx mindist* utility of GROMACS; one atomic contact occurs when the distance between any two atoms in different groups is less than 0.6 nm.

4. Conclusions

We reported a facile method to prepare uniformly dispersed polymer-coated Fe₃O₄ nanozymes. The surface modification of Fe₃O₄ NPs with dopamine allows further functionalization with acryloyl groups. Followed by an in situ polymerization, Fe₃O₄ NPs

were encapsulated in polyacrylamide nanogel. In comparison with the naked Fe_3O_4 NPs, the polymer-coated nanoparticles displayed an enhanced catalytic removal efficiency to a library of organic dyes when using either H_2O_2 or $\text{Na}_2\text{S}_2\text{O}_8$ as primary oxidants. In this study, most dyes were oxidatively removed using as little as 5 mg/L of PAM-coated Fe_3O_4 . The molecular simulation revealed that the coordination interactions of organic dyes, primary oxidants, and the amide groups of polymer nanocapsules could be the key to the enhanced activity of nanozymes. Moreover, the higher removal efficiency using $\text{Na}_2\text{S}_2\text{O}_8$ as the primary oxidant was attributed to the long life of the $\cdot\text{SO}_4^-$ radicals and the stronger interaction between $\text{Na}_2\text{S}_2\text{O}_8$ and the amide groups of PAM, which allows gradual conversion from sulfate radicals to hydroxyl radicals. As such, the PAM-coated Fe_3O_4 in the presence of $\text{Na}_2\text{S}_2\text{O}_8$ demonstrated systematically higher (up to above 90%) catalytic efficiency than those using H_2O_2 (mostly below 10%). While the small particle size resulted in much higher catalytic efficiency with lower catalyst loading, it resulted in the difficulty of catalyst recycling. Future work will focus on immobilizing these nanogels on the micron size carriers for better recyclability. Overall, this work provided insights into the understanding of why specific polymer coating layers could overall improve the catalytic efficiency and may guide the further design of polymer-based nanozyme in different catalytic applications.

Supplementary Materials: The following supporting information can be downloaded at: <https://www.mdpi.com/article/10.3390/catal12060614/s1>, Figure S1: The corresponding elemental mapping pattern of the dried $\text{Fe}_3\text{O}_4@\text{Gel}$; Figure S2: The catalytic degradation of IC using $\text{Fe}_3\text{O}_4@\text{Gel}$ as a nanozyme with various concentrations of H_2O_2 (A) and $\text{Fe}_3\text{O}_4@\text{Gel}$ (B); Figure S3: Influence of pH on the $\text{Fe}_3\text{O}_4@\text{Gel}$ -mediated oxidation of dye pollutant; Figure S4: Influence of various initial parameters on the $\text{Fe}_3\text{O}_4@\text{Gel}$ -mediated oxidation of dye pollutant: (A) $\text{Na}_2\text{S}_2\text{O}_8$ dosage, (B) $\text{Fe}_3\text{O}_4@\text{Gel}$ loading; Table S1: A comparison of catalysis performance between this work and literature that used similar catalysis systems. Refs [40–44] are cited in the Supplementary Materials.

Author Contributions: Conceptualization, Y.C. and Z.J.; methodology, J.Z. and Z.F.; validation, J.Z., W.W. and P.X.; investigation, J.Z. and H.H.; data curation, J.Z.; writing—original draft preparation, W.W. and Y.C.; writing—review and editing, J.Z. and Z.F.; project administration, Y.C.; funding acquisition, Y.C. All authors have read and agreed to the published version of the manuscript.

Funding: This research was funded by Natural Science Foundation of China, grant number 22173061.

Data Availability Statement: Not applicable.

Conflicts of Interest: The authors declare no conflict of interest.

References

1. Boczkaj, G.; Fernandes, A. Wastewater treatment by means of advanced oxidation processes at basic pH conditions: A review. *Chem. Eng. J.* **2017**, *320*, 608–633. [CrossRef]
2. Yan, S.; Zhang, X.; Zhang, H. Persulfate activation by Fe(III) with bioelectricity at acidic and near-neutral pH regimes: Homogeneous versus heterogeneous mechanism. *J. Hazard. Mater.* **2019**, *374*, 92–100. [CrossRef] [PubMed]
3. Xing, M.; Xu, W.; Dong, C.; Bai, Y.; Zeng, J.; Zhou, Y.; Zhang, J.; Yin, Y. Metal Sulfides as Excellent Co-catalysts for H_2O_2 Decomposition in Advanced Oxidation Processes. *Chem* **2018**, *4*, 1359–1372. [CrossRef]
4. Dong, C.; Ji, J.; Shen, B.; Xing, M.; Zhang, J. Enhancement of H_2O_2 Decomposition by the Co-catalytic Effect of WS₂ on the Fenton Reaction for the Synchronous Reduction of Cr(VI) and Remediation of Phenol. *Environ. Sci. Technol.* **2018**, *52*, 11297–11308. [CrossRef] [PubMed]
5. Liang, M.; Yan, X. Nanozymes: From New Concepts, Mechanisms, and Standards to Applications. *Acc. Chem. Res.* **2019**, *52*, 2190–2200. [CrossRef] [PubMed]
6. Bethi, B.; Sonawane, S.H.; Bhanvase, B.A.; Gumfekar, S.P. Nanomaterials-based advanced oxidation processes for wastewater treatment: A review. *Chem. Eng. Process. Process Intensif.* **2016**, *109*, 178–189. [CrossRef]
7. Gao, L.; Zhuang, J.; Nie, L.; Zhang, J.; Zhang, Y.; Gu, N.; Wang, T.; Feng, J.; Yang, D.; Perrett, S.; et al. Intrinsic peroxidase-like activity of ferromagnetic nanoparticles. *Nat. Nanotechnol.* **2007**, *2*, 577–583. [CrossRef]
8. Fan, J.; Gu, L.; Wu, D.; Liu, Z. Mackinawite (FeS) activation of persulfate for the degradation of p-chloroaniline: Surface reaction mechanism and sulfur-mediated cycling of iron species. *Chem. Eng. J.* **2018**, *333*, 657–664. [CrossRef]
9. Wei, Y.; Liu, H.; Liu, C.; Luo, S.; Liu, Y.; Yu, X.; Ma, J.; Yin, K.; Feng, H. Fast and efficient removal of As(III) from water by CuFe_2O_4 with peroxydisulfate: Effects of oxidation and adsorption. *Water Res.* **2019**, *150*, 182–190. [CrossRef]

10. Li, Z.; Yang, X.; Yang, Y.; Tan, Y.; He, Y.; Liu, M.; Liu, X.; Yuan, Q. Peroxidase-Mimicking Nanozyme with Enhanced Activity and High Stability based on Metal-Support Interaction. *Chemistry* **2017**, *24*, 409–415. [\[CrossRef\]](#)
11. Pan, F.; Ji, H.; Du, P.; Huang, T.; Wang, C.; Liu, W. Insights into catalytic activation of peroxymonosulfate for carbamazepine degradation by MnO₂ nanoparticles in-situ anchored titanate nanotubes: Mechanism, ecotoxicity and DFT study. *J. Hazard. Mater.* **2021**, *402*, 123779. [\[CrossRef\]](#) [\[PubMed\]](#)
12. Shen, Y.; Zhang, Y.; Zhang, X.; Zhou, X.; Teng, X.; Yan, M.; Bi, H. Horseradish peroxidase-immobilized magnetic mesoporous silica nanoparticles as a potential candidate to eliminate intracellular reactive oxygen species. *Nanoscale* **2015**, *7*, 2941–2950. [\[CrossRef\]](#) [\[PubMed\]](#)
13. Lei, Y.; Chen, C.S.; Tu, Y.J.; Huang, Y.H.; Zhang, H. Heterogeneous Degradation of Organic Pollutants by Persulfate Activated by CuO-Fe₃O₄: Mechanism, Stability, and Effects of pH and Bicarbonate Ions. *Environ. Sci. Technol.* **2015**, *49*, 6838–6845. [\[CrossRef\]](#) [\[PubMed\]](#)
14. Zhou, R.; Shen, N.; Zhao, J.; Su, Y.; Ren, H. Glutathione-coated Fe₃O₄ nanoparticles with enhanced Fenton-like activity at neutral pH for degrading 2,4-dichlorophenol. *J. Mater. Chem. A* **2018**, *6*, 1275–1283. [\[CrossRef\]](#)
15. Liu, J.; Zhou, J.; Ding, Z.; Zhao, Z.; Xu, X.; Fang, Z. Ultrasound irradiation enhanced heterogeneous activation of peroxymonosulfate with Fe₃O₄ for degradation of azo dye. *Ultrason. Sonochem.* **2017**, *34*, 953–959. [\[CrossRef\]](#)
16. Sun, C.; Zhou, R.; E, J.; Sun, J.; Su, Y.; Ren, H. Ascorbic acid-coated Fe₃O₄ nanoparticles as a novel heterogeneous catalyst of persulfate for improving the degradation of 2,4-dichlorophenol. *RSC Adv.* **2016**, *6*, 10633–10640. [\[CrossRef\]](#)
17. He, L.; Li, M.-X.; Chen, F.; Yang, S.-S.; Ding, J.; Ding, L.; Ren, N.-Q. Novel coagulation waste-based Fe-containing carbonaceous catalyst as peroxymonosulfate activator for pollutants degradation: Role of ROS and electron transfer pathway. *J. Hazard. Mater.* **2021**, *417*, 126113. [\[CrossRef\]](#)
18. Xiao, S.; Cheng, M.; Zhong, H.; Liu, Z.F.; Liu, Y.; Yang, X.; Liang, Q.H. Iron-mediated activation of persulfate and peroxymonosulfate in both homogeneous and heterogeneous ways: A review. *Chem. Eng. J.* **2020**, *384*, 123265. [\[CrossRef\]](#)
19. Liu, B.; Liu, J. Surface modification of nanozymes. *Nano Res.* **2017**, *10*, 1125–1148. [\[CrossRef\]](#)
20. An, P.; Zuo, F.; Wu, Y.P.; Zhang, J.H.; Zheng, Z.H.; Ding, X.B.; Peng, Y.X. Fast synthesis of dopamine-coated Fe₃O₄ nanoparticles through ligand-exchange method. *Chin. Chem. Lett.* **2012**, *23*, 1099–1102. [\[CrossRef\]](#)
21. Xie, Y.; Yan, B.; Xu, H.; Chen, J.; Liu, Q.; Deng, Y.; Zeng, H. Highly regenerable mussel-inspired Fe(3)O(4)@polydopamine-Ag core-shell microspheres as catalyst and adsorbent for methylene blue removal. *ACS Appl Mater. Interfaces* **2014**, *6*, 8845–8852. [\[CrossRef\]](#) [\[PubMed\]](#)
22. Zhang, Z.; Zhang, X.; Liu, B.; Liu, J. Molecular Imprinting on Inorganic Nanozymes for Hundred-fold Enzyme Specificity. *J. Am. Chem. Soc.* **2017**, *139*, 5412–5419. [\[CrossRef\]](#) [\[PubMed\]](#)
23. Chen, C.; Sun, W.; Lv, H.; Li, H.; Wang, Y.; Wang, P. Spacer arm-facilitated tethering of laccase on magnetic polydopamine nanoparticles for efficient biocatalytic water treatment. *Chem. Eng. J.* **2018**, *350*, 949–959. [\[CrossRef\]](#)
24. Xiao, F.; Xiao, P.; Jiang, W.; Wang, D. Immobilization of horseradish peroxidase on Fe₃O₄ nanoparticles for enzymatic removal of endocrine disrupting chemicals. *Environ. Sci. Pollut. Res. Int.* **2020**, *27*, 24357–24368. [\[CrossRef\]](#)
25. Li, Z.; Chen, Z.; Zhu, Q.; Song, J.; Li, S.; Liu, X. Improved performance of immobilized laccase on Fe₃O₄@C-Cu²⁺ nanoparticles and its application for biodegradation of dyes. *J. Hazard. Mater.* **2020**, *399*, 123088. [\[CrossRef\]](#)
26. Liu, S.; Huang, B.; Zheng, G.; Zhang, P.; Li, J.; Yang, B.; Chen, Y.T.; Liang, L. Nanocapsulation of horseradish peroxidase (HRP) enhances enzymatic performance in removing phenolic compounds. *Int. J. Biol. Macromol.* **2020**, *150*, 814–822. [\[CrossRef\]](#)
27. Zheng, G.; Liu, S.; Zha, J.; Zhang, P.; Xu, X.; Chen, Y.; Jiang, S. Protecting Enzymatic Activity via Zwitterionic Nanocapsulation for the Removal of Phenol Compound from Wastewater. *Langmuir* **2019**, *35*, 1858–1863. [\[CrossRef\]](#)
28. Tan, C.; Gao, N.; Deng, Y.; Deng, J.; Zhou, S.; Li, J.; Xin, X. Radical induced degradation of acetaminophen with Fe₃O₄ magnetic nanoparticles as heterogeneous activator of peroxymonosulfate. *J. Hazard. Mater.* **2014**, *276*, 452–460. [\[CrossRef\]](#)
29. De Laat, J.; Dao, Y.H.; El Najjar, N.H.; Daou, C. Effect of some parameters on the rate of the catalysed decomposition of hydrogen peroxide by iron(III)-nitrilotriacetate in water. *Water Res.* **2011**, *45*, 5654–5664. [\[CrossRef\]](#)
30. Guo, J.; Liu, Y.; Zha, J.; Han, H.; Chen, Y.; Jia, Z. Enhancing the peroxidase-mimicking activity of hemin by covalent immobilization in polymer nanogels. *Polym. Chem.* **2021**, *12*, 858–866. [\[CrossRef\]](#)
31. Oh, W.-D.; Dong, Z.; Lim, T.-T. Generation of sulfate radical through heterogeneous catalysis for organic contaminants removal: Current development, challenges and prospects. *Appl. Catal. B Environ.* **2016**, *194*, 169–201. [\[CrossRef\]](#)
32. Liu, Z.L.; Wang, H.B.; Lu, Q.H.; Du, G.H.; Peng, L.; Du, Y.Q.; Zhang, S.M.; Yao, K.L. Synthesis and characterization of ultrafine well-dispersed magnetic nanoparticles. *J. Magn. Magn. Mater.* **2004**, *283*, 258–262. [\[CrossRef\]](#)
33. Ghosh, R.; Pradhan, L.; Devi, Y.P.; Meena, S.S.; Tewari, R.; Kumar, A.; Sharma, S.; Gajbhiye, N.S.; Vatsa, R.K.; Pandey, B.N.; et al. Induction heating studies of Fe₃O₄ magnetic nanoparticles capped with oleic acid and polyethylene glycol for hyperthermia. *J. Mater. Chem.* **2011**, *21*, 13388–13398. [\[CrossRef\]](#)
34. Cheng, H.; Zhang, L.; He, J.; Guo, W.; Zhou, Z.; Zhang, X.; Nie, S.; Wei, H. Integrated Nanozymes with Nanoscale Proximity for in Vivo Neurochemical Monitoring in Living Brains. *Anal. Chem.* **2016**, *88*, 5489–5497. [\[CrossRef\]](#) [\[PubMed\]](#)
35. Malde, A.K.; Zuo, L.; Breeze, M.; Stroet, M.; Poger, D.; Nair, P.C.; Oostenbrink, C.; Mark, A.E. An Automated Force Field Topology Builder (ATB) and Repository: Version 1.0. *J. Chem. Theory Comput.* **2011**, *7*, 4026–4037. [\[CrossRef\]](#) [\[PubMed\]](#)
36. Reif, M.M.; Hunenberger, P.H.; Oostenbrink, C. New Interaction Parameters for Charged Amino Acid Side Chains in the GROMOS Force Field. *J. Chem. Theory Comput.* **2012**, *8*, 3705–3723. [\[CrossRef\]](#) [\[PubMed\]](#)

37. Jorgensen, W.L.; Chandrasekhar, J.; Madura, J.D.; Impey, R.W.; Klein, M.L. Comparison of Simple Potential Functions for Simulating Liquid Water. *J. Chem. Phys.* **1983**, *79*, 926–935. [[CrossRef](#)]
38. Pronk, S.; Pall, S.; Schulz, R.; Larsson, P.; Bjelkmar, P.; Apostolov, R.; Shirts, M.R.; Smith, J.C.; Kasson, P.M.; van der Spoel, D.; et al. GROMACS 4.5: A high-throughput and highly parallel open source molecular simulation toolkit. *Bioinformatics* **2013**, *29*, 845–854. [[CrossRef](#)]
39. DeLano, W.L. *The PyMOL Molecular Graphics System*; DeLano Scientific: San Carlos, CA, USA, 2002.
40. Jacinto, M.J.; Souto, R.S.; Silva, V.C.P.; Prescilio, I.C.; Kauffmann, A.C.; Soares, M.A.; de Souza, J.R.; Bakuzis, A.F.; Fontana, L.C. Biosynthesis of Cube-Shaped Fe₃O₄ Nanoparticles for Removal of Dyes Using Fenton Process. *Water Air Soil Pollut.* **2021**, *232*, 270. [[CrossRef](#)]
41. Kang, Y.-G.; Yoon, H.; Lee, C.-S.; Kim, E.-J.; Chang, Y.-S. Advanced oxidation and adsorptive bubble separation of dyes using MnO₂-coated Fe₃O₄ nanocomposite. *Water Res.* **2019**, *151*, 413–422. [[CrossRef](#)]
42. Yang, R.; Peng, Q.; Yu, B.; Shen, Y.; Cong, H. Yolk-shell Fe₃O₄@MOF-5 nanocomposites as a heterogeneous Fenton-like catalyst for organic dye removal. *Sep. Purif. Technol.* **2021**, *267*, 118620. [[CrossRef](#)]
43. Li, K.; Zhao, Y.; Song, C.; Guo, X. Magnetic ordered mesoporous Fe₃O₄/CeO₂ composites with synergy of adsorption and Fenton catalysis. *Appl. Surf. Sci.* **2017**, *425*, 526–534. [[CrossRef](#)]
44. Li, W.; Wu, X.; Li, S.; Tang, W.; Chen, Y. Magnetic porous Fe₃O₄/carbon octahedra derived from iron-based metal-organic framework as heterogeneous Fenton-like catalyst. *Appl. Surf. Sci.* **2018**, *436*, 252–262. [[CrossRef](#)]